ELSEVIER

Biophysical Chemistry 79 (1999) 163–186

Biophysical Chemistry

Letter

Complex patterns predicted in an in vitro experimental model system for the evolution of molecular cooperation

T. Kirner*, J. Ackermann, R. Ehricht, J.S. McCaskill

Department of Molecular Information Processing, Institute of Molecular Biotechnology (IMB), Beutenbergstr. 11, D-07745 Jena, Germany

Received 15 November 1998; received in revised form 28 January 1999; accepted 19 March 1999

Abstract

An isothermal biochemical in vitro amplification system with two trans-cooperatively coupled amplifying DNA molecules was investigated homogeneously using a hierarchy of kinetic models and as a simplified reaction–diffusion system. In our model of this recently developed experimental system, no reaction mechanism higher than second order occurs, yet numerical simulations show a variety of complex spatiotemporal patterns which arise in response to finite amplitude perturbations in a flow reactor. In a certain domain of the kinetic parameters the system shows self-replicating spots. These spots can stabilize the cooperative amplification in such evolving systems against emerging parasites. The results are of high relevance for experimental studies on these functional in vitro ecosystems in spatially resolved microstructured reactors.

Keywords: DNA; Pattern formation; Reaction–diffusion; Self-replicating spots; Molecular evolution; Coevolution; Cooperation

1. Introduction

Part of the interest in pattern forming chemical systems is that, at least since Turing's pioneering work [1], they have provided model systems for biological pattern formation. Examples of pattern formation in chemical reactions are the waves in the Belousov–Zhabotinskii reaction [2,3], the stationary patterns in the chloride-iodide-malonic acid reaction [4,5] and the spatiotemporal patterns formed in the process of heterogeneous catalysis [6]. Unlike some of their biological counterparts, however, these pattern forming systems are not capable of evolution. Following much

* Corresponding author. Fax: +49-3641-65-6191.
E-mail address: tkirner@imb-jnea.de (T. Kirner)

0301-4622/99/$ - see front matter
PII: S0301-4622(99)00049-6

work on the Belousov–Zhabotinskii reaction [7], interest has been rekindled by the observation of cell like patterns in the ferrocyanide-iodate-sulfite reaction [8] after their prediction as 'self-replicating spots' in the Gray–Scott model [9].

In vitro system exhibiting molecular evolution, on the other hand, have to date belonged to the class of multicomponent exponential amplification (biochemical) systems with saturation, such as the Qβ replicase system [10], the strand replacement reaction [11], the 3SR reaction [12–14] or the polymerase chain reaction (PCR) [15,16]. The parabolic class of enzyme-free template assembly catalyzed self-replicating systems such as the hexanucleotide system of von Kiedrowski [17], the 'naphthalene' system of Rebek [18], or the peptide system of Ghadiri [19] although showing a moderate degree of combinatorial coexistence, have not yet been demonstrated to exhibit significant evolution. Spatial pattern formation in these systems has been limited to the demonstration of Fisher waves in the Qβ [20,21] and the 3SR [22] reactions in one-, two- or three-dimensions. The authors have observed the evolution of wavefront velocities through sequence changes in these systems. Complex pattern formation like self-replicating spots is not expected, however, since the necessary non-linearity in the autocatalytic terms is absent.

More recent, however, two in vitro model ecological systems based on the 3SR reaction have been constructed: a predator–prey system [23] and a symbiotic or cooperatively coupled system (CATCH) [24] in which non-linear interactions of the quadratic type occur. These systems allow direct molecular evolution, which can be followed by DNA sequencing, and because of their non-linear interactions they may allow some degree of pattern formation when placed in a spatially resolved but chemically open microenvironment. Such spatial microenvironments have been constructed using micromachining technology in silicon and pyrex glass in one- or two-dimensions [25] in our laboratory. These reactors had to be developed to work with much smaller volumes than usual in the area of reaction diffusion systems [4,26]. Whereas previous theoretical work has demonstrated that kinetically realistic models of the predator–prey system exhibit chemical oscillations in homogeneously mixed flow reactors [27], the present work focuses on the symbiotic model system CATCH and explores the kinetic features and spatial pattern forming potential of this experimental system.

The evolutionary significance of the self-replicating spot pattern was first recorded in McCaskill [28] and studied for abstract models [29,30] of the spatial stabilization of molecular cooperation against (destructive) exploitation. Spatial isolation has been seen as a necessary feature for a wide range of models for the origin and maintenance of cooperation. In the population genetics literature, cooperative or altruistic alleles (cooperation is rarely without some cost to the individuals, at least relative to variants which exploit the positive features of the cooperator) can survive in structured populations such as Wright's island model [31,32] as studied for example by Kimura and Aoki [33,34] and utilized by Dyson in his model for the origin of the genetic code [35]. Dividing compartments, as found in cells, are not essential for this stabilization, but it is a relatively weak effect because of stochastic fluctuations in the membership of compartments. Szathmary has popularized the positive effect of compartments as the stochastic-corrector model [36]. The problem of molecular cooperation was addressed by several authors at the beginning of the 1970s as a key problem in the origin of life [37–39]. Eigen's hypercycle concept was designed to overcome the limited information acquisition of error-prone copying systems by catalytically coupling replicators in a closed cycle, but requires some form of compartments to avoid generic parasitic exploitation [40–42]. The discovery that hypercycles could be stabilized against parasites in spatially extended systems by the self-generation of spiral wave reaction–diffusion patterns [43] was a major step forward in our understanding of incipient cooperation. It requires, however, a rather improbable emergence of a five or more member hypercycle to create the evolutionary stable spiral patterns.

The existence of a much simpler experimental cooperative structure CATCH consequently prompts an analysis of its pattern forming poten-

tial. CATCH has recently been found to evolve to a simple two-member hypercycle-like structure (but with different kinetics from the replicator equation) [44] in serial transfer experiments. In this work we demonstrate that detailed kinetic models, and a hierarchy of simplified schemes which captures essential features of the kinetics, exhibit spatial patterns including the self-replicating spot patterns (previously found to require a third order reaction step) which can potentially be useful in stabilizing the molecular cooperation against evolving exploitation. While a stochastic treatment is necessary for the latter problem, we investigate the kinetics and pattern formation in this paper using deterministic kinetics and reaction–diffusion equations.

The aim of this work is to study if the CATCH system is able to show spatiotemporal patterns in an open two-dimensional reactor under the appropriate choice of experimental conditions. The dimension of the parameter space which can be varied in such experiments is rather large. The flow rate and the concentrations of the primers and enzymes in the inflow can be chosen independently. The dimensions of the (microstructured) reactor will play a crucial role. The reaction rates may also be influenced by the choice of DNA sequences or the pH value of the solvent for example. Specific death reactions may be introduced by adding enzymes like RNase or DNase.

In Section 2, the cooperatively coupled amplification system is modeled in terms of simplifying reaction steps. Solving the corresponding reaction–diffusion system for a certain choice of the parameters would tell us if pattern formation could occur there. Such a simulation for the extended reaction system is time consuming because the numbers of species involved is rather large and the reaction system is numerically stiff. Finding a suitable set of parameters for pattern formation by random test may be extremely unlikely. Moreover, a better understanding of the basis mechanism responsible for the pattern formation is desirable to allow the simulation to be transferred to experimental situations.

We will treat this problem in a classical way. In Section 3, the derived homogeneous reaction system will be reduced to a hierarchy of small reaction systems. To motivate the reduction, we choose specific experimental conditions (resources and primers in excess, a certain dynamical range of concentrations) for which the kinetics of the full system and that of the reduced system are equivalent. The kinetic behavior of the systems will be compared and discussed in Section 4.

A bifurcation analysis for the reduced systems will be presented in Section 5. The Hopf bifurcation occurring for certain choices of the parameters indicates in which parameter regions pattern formation can be expected. The results of numerical simulation of the reaction–diffusion equation in Section 6 will show which patterns if any occur. The relevance of the theoretical results for experiments will be discussed in Section 7.

2. The model

In vitro amplification of biologically important nucleic acids such as RNA and DNA molecules usually involves the *p*olymerase *c*hain *r*eaction (PCR) [15,16]. This synchronized amplification method consists of multiple temperature cycles of oligonucleotide primer-directed DNA replication with a thermostable DNA polymerase. In contrast, the amplification system on which our model is based is isothermal, the self-sustained sequence replication (3SR) reaction [12–14], also known as *n*ucleic *a*cid *s*equence-*b*ased *a*mplification (NASBA) [45,46]. A target nucleic acid sequence replicates exponentially using the three enzymes reverse transcriptase (RT), ribonuclease (RNaseH), and DNA-dependent RNA polymerase (transcription) [13]. Two DNA primers (P_1 and P_2) must be provided at relatively high concentrations and their sequences may be used to guide the amplification process. The essential amplification step involves the repeated process of RNA transcription from the double-stranded template (dsDNA), whereas the RNA is consumed in the ensuing process of reconversion to double stranded (ds) DNA by reverse transcription. The absence of thermally synchronized cycling allows spatially distributed systems to be studied free from the complications of thermal expansion and convective mixing [21]. To investi-

gate evolving molecular cooperation, an experimental system has been constructed in which the amplification of two molecular species is coupled trans-cooperatively [24]. The overall coupling scheme of the CATCH system is shown in Fig. 1. These species are single-stranded (ss) DNA templates (DNA_1 and DNA_2). Coupling occurs if DNA_1 and DNA_2 anneal to each other via a (reverse) complementary region (DB and DB′) situated at the 3′ end of each template. RT elongates the hybridized templates producing a double-stranded DNA (see Fig. 2a). This double strand contains two promoters, which are located on either side of and directly adjacent to DB, and which are oriented towards each other. These promoters specify two RNA transcripts (Fig. 2b) which revert to DNA_1 and DNA_2 after hybridization of the two primers (P_1 and P_2) and reverse transcription (Fig. 2c).

This *c*ooperative *a*mplification of *t*emplates by *c*ross-*h*ybridization (CATCH) [24] is trans-cooperative according to the promoter function. The amplification ability of DNA_1 depends on the promoter sequence embedded in DNA_2 and vice versa. Lethal mutations in the promoter regions are thus inevitably emerging parasites: they only

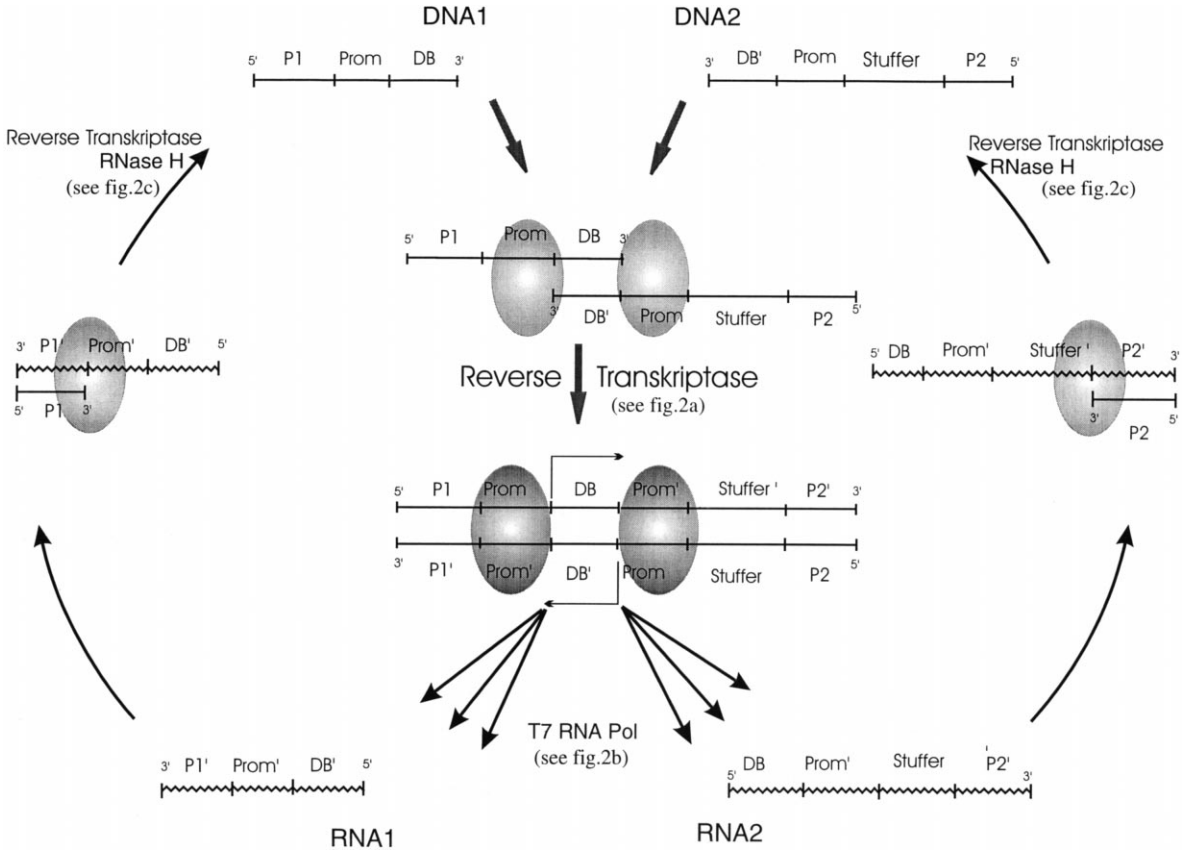

Fig. 1. Reaction scheme for the 'cooperative amplification of templates by cross-hybridization' (CATCH) system. The amplification cycles of RNA_1 and RNA_2 are coupled cooperatively via a common double stranded DNA intermediate. The amplification cycle starts with the hybridization of the corresponding primers P_1 and P_2 to RNA_1 and RNA_2, respectively. Reverse transcription and digestion of the RNA by RNaseH leads to the single stranded species DNA_1 and DNA_2. The 3′ termini of DNA_1 and DNA_2 are able to base pair in the complementary region DB and are elongated by reverse transcriptase producing a double stranded DNA. This double stranded DNA contains two promoters for a DNA dependent RNA polymerase, on either side of the DB region and oriented towards each other. Starting at these promoter sequences RNA_1 and RNA_2 are regenerated in multiple copies by transcription.

receive cooperative support from without serving as an amplification module for the coupled species. Another possible type of primer exploitation arises if self-priming in the DB region occurs [47]. Some kind of kinetic or evolutionary stabilization against parasitic species is indispensable for the long term evolution of cooperation. As mentioned in Section 1, one of the authors has proposed that the spatiotemporal patterns of self-replicating spots can provide a solution. Some form of spatial structuring appears necessary in all known examples of the stabiliza-

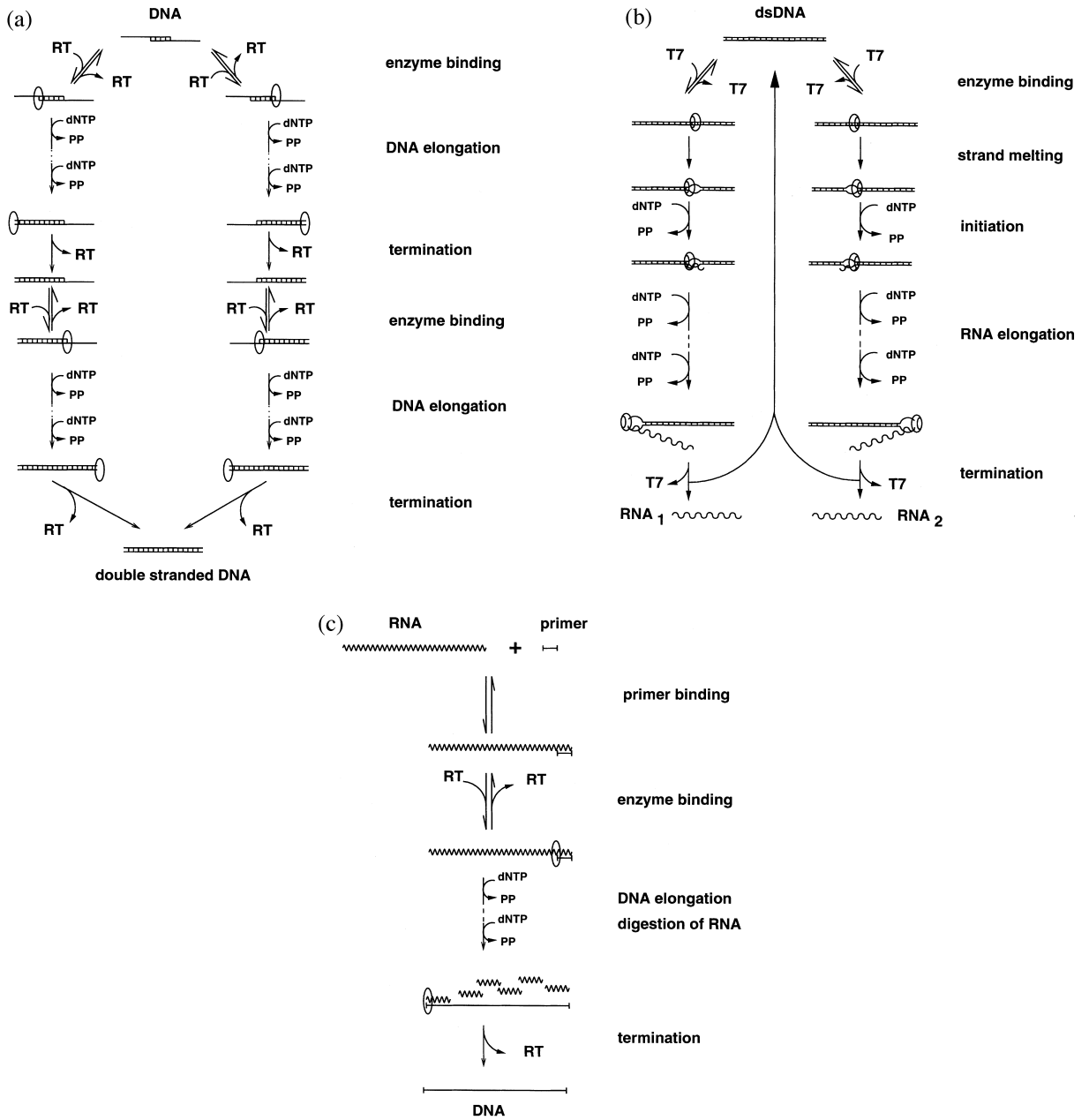

Fig. 2.

tion of cooperation in the presence of parasites. Therefore the search for a system inherent property of pattern formation appears important as a condition for the evolutionary stability of the biochemical CATCH system.

The enzymatic amplification process of the CATCH system described above consists of a sequence of rather complicated biochemical processes. We model the system in terms of simplifying chemical reaction steps seeking to provide sufficient detail to ensure the broad applicability of our results, and not to provide the last word on the kinetics of the 3SR reaction.

2.1. The essential non-linear step

After the annealing of two single-stranded (ss) DNA templates (DNA_1 and DNA_2) to a DNA_{12} complex:

$$DNA_1 + DNA_2 \xrightarrow{k_1} DNA_{12}, \tag{1}$$

the reverse transcriptase (RT) binds to the DNA_{12} complex and consumes dNTPs (deoxyribonucleotide triphosphate) to elongate the complex to a double stranded DNA (dsDNA).

$$\begin{aligned} DNA_{12} + RT &\xrightarrow{k_2} DNA_{12}{:}RT \\ DNA_{12}{:}RT + n \times dNTP &\xrightarrow{k_3} dsDNA + RT. \end{aligned} \tag{2}$$

This process is vastly simplified here. The reverse transcriptase can bind in two different ways to the DNA complex, one for each direction of double strand completion. An initiation step may have to take place. At any stage of the process the probability for the dissociation of the enzyme is non-zero, reflecting the finite processivity of RT, with elongation proceeding when a RT enzyme has bound to the DNA complex again. Two enzymes may act simultaneously on the strand. The rate of each process depends on the sequence (and folding structure) of the template. A slow dissociation of the enzyme–template complex may be the rate limiting step for the whole process. The incorporation of all nucleotides are modeled by one reaction step and an effective nucleotide concentration [dNTP] is used to take the exhaustion of nucleotides into account. The kinetics of the nucleotide incorporation have been extensively studied [48–59]. In an amplification cycle, as studied here, incomplete elongation will lead to a large diversity of species, which may interact with one another and be further processed by the enzymes. Such sequence specific effects are out of the scope of a theoretical modeling in terms of ordinary and partial differential equations on which we will concentrate in this work. A framework for a proper evolutionary stochastic treatment has been discussed elsewhere [29]. These restrictions also apply to our modeling of the other reaction steps even if we do not repeat this discussion below. For experimentally measured kinetic rate constants we refer to Table 2 and the literature listed there.

Fig. 2. Kinetic mechanism for individual enzymes: (a) DNA-dependent DNA polymerase of HIV reverse transcriptase (RT). The process starts with the reversible binding of RT to the DNA template: template complex. Binding take place at two sites on the DNA complex, followed by polymerization from $3 \rightarrow 5'$ elongating the single strands to the end of the opposing templated strand. Deoxyribonucleotide triphosphates (dNTP) are incorporated during this process and pyrophosphates (PP) are produced. After complete elongation in one direction, the enzyme dissociates from the partly double stranded DNA and the processes binding of RT, polymerization, and termination is repeated to complete the double stranded DNA. (b) Double stranded DNA dependent T7 RNA polymerase. The processes of RNA transcription involves several stages: reversible binding of T7, melting of the double stranded DNA, initiation of transcription, processive RNA transcription and termination. Ribonucleotide triphosphates (rNTP) are incorporated during this process and pyrophosphates (PP) are produced. The regeneration of double stranded DNA is responsible for the net amplification of the CATCH and 3SR cycles. (c) RNA-dependent DNA polymerase of HIV reverse transcriptase (RT). The process starts with the reversible binding of the DNA primer to the RNA template. HIV reverse transcriptase binds to the template:primer complex followed by DNA polymerization. The RNAseH activity of the HIV reverse transcriptase is responsible for the digestion of the RNA. Deoxyribonucleotide triphosphates (dNTP) are incorporated during the transcription and pyrophosphates (PP) are produced. After complete polymerization the enzyme dissociates from the single stranded DNA.

Table 1
Concentrations of enzymes, primer, and nucleotides in the inlet and the diffusion coefficients of species in the CATCH system as employed in the numerical simulations[a]

Parameter	Value	
Concentrations		
rt_{in}	1×10^{-6} M	Reverse transcriptase enzyme
t_{in}	1×10^{-6} M	Transcriptase enzyme
p_{in}	2×10^{-6} M	Primer concentrations
m_{in}	1×10^{-6} M	Effective rNTP concentration
d_{in}	4×10^{-5} M	Effective dNTP concentration
Diffusion rates		
D_1	2×10^{-7} cm^2 s^{-1}	Polynucleotides (average value)
D_2	4×10^{-7} cm^2 s^{-1}	Nucleotides

[a]*Notes.* The (effective) nucleotide concentrations gives the concentration of polynucleotides which can be amplified by consuming all nucleotides and neglecting abortive products [see Eq. (6) and following]. In the experiments it will be best to give three nucleotides in excess (>0.2 mM) and one nucleotide (UTP for example) below its K_m value (see Table 3). The diffusion coefficients for the nucleotides are chosen twice as large as the diffusion coefficients of the polynucleotides, in practice this difference is even larger. For a more detailed discussion of the process see the cited literature and literature therein.

2.2. RNA transcription

The double stranded DNA (dsDNA) contains two double stranded promoters which provide starting points for RNA transcription by the polymerase T. The polymerase binds to these promoter regions

$$\mathrm{dsDNA} + \mathrm{T} \overset{k_4}{\rightarrow} \mathrm{dsDNA{:}T} \tag{3}$$

and initiates DNA-dependent RNA polymerization

$$\mathrm{dsDNA{:}T} + n \times \mathrm{rNTP} \overset{k_5}{\rightarrow} \mathrm{dsDNA} + \mathrm{T} + \mathrm{RNA}_1 + \mathrm{RNA}_2 . \tag{4}$$

RNA nucleotides are consumed during the RNA-polymerization. Early experiments on the T7 family of DNA-dependent RNA polymerase showed that the promoter-enzyme binding followed by transcription can be fitted well to the pre-steady state kinetics [60–64] if the nucleotide concentrations are sufficiently high (>0.2 mM). RNA transcription, described above by k_5, includes complicated processes: melting of the double stranded DNA, initiation of transcription, processive elongation and termination. The rate limiting step is the initiation of transcription, but the dependence of all of these steps on the nucleotide concentration has (to our knowledge) not been completely elucidated experimentally. However, a variation of the nucleotide concentration leads to a variation of the overall rate of T7 RNA synthesis which can be fitted to a Michaelis–Menten kinetics [65]. The values of the Michaelis–Menten constant depend on the type of nucleotides (ATP, GTP, UTP, and CTP). We propose to use experimental nucleotide concentrations much smaller than these K_m values, in which case the DNA-dependent RNA-polymerase of the T7-enzyme can be modeled as above by a second order (nucleotide consuming) reaction, see Section 3 for a discussion. For a more detailed discussion of the kinetic rate constants and modeling of the T7 RNA polymerase we refer to Table 3 and the literature listed there.

2.3. Reverse transcription

Primers P_1 and P_2 hybridize to RNA_1 and RNA_2, respectively. Binding and reverse transcription by RT leads to the two starting single-stranded DNA strands (DNA_1 and DNA_2)

Table 2
List of experimental kinetic data measured for the DNA-dependent DNA polymerase function of HIV reverse transcriptase (RT) following binding of RT to DNA template/primers:[a]

$$\mathrm{RT} + \mathrm{DNA}_1{:}\mathrm{DNA}_2 \underset{k_{-2}}{\overset{k_2}{\rightleftharpoons}} \mathrm{DNA}_1{:}\mathrm{DNA}_2{:}\mathrm{RT} \overset{\tilde{k}_3}{\rightarrow} \mathrm{dsDNA} + \mathrm{RT}$$

Parameter	Value	References
DNA–DNA binding rate		
k_1 (M^{-1} s^{-1})	$10^{7 \pm 1}$[b]	20/20-mer [94]
$K_d^{(1)}$ (nM)	7–25	CATCH system [95]
Binding of HIV reverse transcriptase (RT) enzyme to DNA / DNA complex		
k_2 (M^{-1} s^{-1})	2.3×10^6	23/32-mer [56]
	2.0×10^8	19/32-mer [96]
$K_d^{(2)}$ (nM)	4.7	25/45-mer [51]
	26	23/32-mer [56]
	26–500[c]	19/32-mer [96]
DNA-dependent DNA polymerase of RT		
$\tilde{k}_3 \approx k_{\mathrm{off}}$ (s^{-1})	0.18	25/45-mer [51]
	0.11	23/32-mer [56]
	1.4	19/32-mer [96]
Nucleotide incorporation		
$K_d^{(3)}$ (μM)	4	dATP [51]
	18	dTTP [56]

[a] *Notes.* Subsequent turnover was limited by the rate of dissociation of the product dsDNA from the enzyme. In the CATCH system, the enzymes have to bind in two directions to elongate each of the two opposite open 3′ ends, but both directions can be synthesized by two reverse transcriptase enzymes simultaneously. For a more detailed discussion of the process see the cited literature.
[b] At a temperature of 42°C.
[c] Dependent on the concentration of Mg^{2+}.

$$\begin{aligned}
\mathrm{RNA}_i + \mathrm{P}_i &\overset{k_6}{\rightarrow} \mathrm{RNA}_i{:}\mathrm{P}_i \\
\mathrm{RNA}_i{:}\mathrm{P}_i + \mathrm{RT} &\overset{k_7}{\rightarrow} \mathrm{RNA}_i{:}\mathrm{P}_i{:}\mathrm{RT} \\
\mathrm{RNA}_i{:}\mathrm{P}_i{:}\mathrm{RT} + n \times \mathrm{dNTP} &\overset{k_8}{\rightarrow} \\
\mathrm{DNA}_i + \mathrm{RT}\ (i = 1,2) &
\end{aligned} \tag{5}$$

with DNA-nucleotides being consumed during reverse transcription, closing the amplification cycle by producing the single stranded DNA templates DNA_1 and DNA_2. Since the transcription of RNA [Eq. (4)] can occur repeatedly for each double stranded DNA, several such copies of DNA_1 and DNA_2 are produced by the primer directed reverse transcription [Eq. (5)]. Experimental rate constants for the RNA-directed DNA polymerase of RT are given in Table 4.

To model the necessary flow reactor setting, the following terms must be added:

$$C \overset{F}{\rightarrow} \emptyset \quad \text{for } C \in \mathscr{M}$$

$$\emptyset \overset{F[C]_{in}}{\longrightarrow} C \quad \text{for } C \in \{\mathrm{P}_1, \mathrm{P}_2, \mathrm{RT}, \mathrm{T}\}.$$

$\mathscr{M}$ is the set of all chemical species involved in the reaction scheme, $\emptyset$ is the null species, the constant F is the (volume) flow rate and $[C]_{in}$ the concentration of a certain species in the influx.

3. Hierarchy of models

The dynamics of the system described above depends crucially on the initial concentrations

Table 3
List of experimental kinetic data measured for the double stranded DNA-dependent T7 RNA polymerase[a]

Parameter	Value	References
T7 RNA polymerase–promoter interaction		
k_4 (10^7 M^{-1} s^{-1})	1–10	[97]
	3.9	[98]
k_{-4} (s^{-1})	0.48	[98]
$K_m^{(4)}$ (nM)	20	[60]
	22	[61]
	2	[62]
	1–3	[63]
	2	[64]
k_{cat} (s^{-1})	0.8	[60]
	1.1	[61]
	0.5	[62,63]
	0.47	[64,98]
Nucleotide triphosphate incorporation		
$K_m^{(5)}$ (μM)	47	ATP [65]
	160	GTP [65]
	60	UTP [65]
	114	UTP [99]
	81	CTP [65]
	133	CTP [99]
k_5 (M^{-1} s^{-1})	2.5×10^5[b]	

[a] *Notes.* Early experiments on the T7 family of DNA-dependent RNA polymerase have shown that the promoter–enzyme binding followed by transcription can be fully fitted to the pre-steady state kinetics [60–64]:

$$\text{dsDNA} + \text{T7} \underset{k_{-4}}{\overset{k_4}{\rightleftharpoons}} \text{dsDNA:T7} \overset{k_{cat}}{\rightarrow} \text{dsDNA} + \text{T7} + \text{RNA}$$

if the nucleotide concentrations are sufficient high (> 0.2 mM). The values for the Michaelis–Menten constant $K_m = (k_{-4} + k_{cat})/k_4$ and k_{cat} range from 1–30 nM and 0.4–1.0 s^{-1}, respectively. Under optimized solution conditions a value of $K_m = 1$–3 nM is appropriate. Recently the dissociation constant has been measured to be identical with K_m, while stop flow assay measured association $k_4 = 3$–7×10^7 M^{-1} s^{-1} and dissociation $k_{-4} = 0.2$ s^{-1} for optimized solution conditions [98]. We propose enzyme concentrations far above this value of K_m ($t_{in} = 10^{-4}$ M, see Table 1) and therefore, the assumption that all dsDNAs are bound to enzymes is a good approximation. The processes of RNA transcription described above by k_{cat} includes complicated processes: melting of the double stranded DNA, initiation of transcription, processive elongation and termination. The rate limiting step is the initiation of transcription. Variation of the nucleotide concentration leads to a variation of the overall rate of T7 RNA synthesis which can be fitted to a Michaelis–Menten kinetics [65]. The values K_m depend on the type of nucleotides and the experimental values for ATP, GTP, UTP, and CTP were 4.7, 16, 6 and 8.1×10^{-5} M, respectively. Note that the nucleotide concentration in Table 1 are given in units of the RNA concentration which can be synthesized by consuming all nucleotides (neglecting abortive products). For a chain length of 100 nucleotides and equally distributed nucleotides in the sequence we get $[\text{ATP}]_{in} \approx [\text{GTP}]_{in} \approx [\text{UTP}]_{in} \approx [\text{CTP}]_{in} \approx 25 \times m_{in} = 2.5 \times 10^{-5}$ M. In this case, the RNA synthesis can be described by the second order equation $d[\text{RNA}]/dt \approx k_{cat}/K_m[\text{dsDNA:T7}]\ [\text{rNTP}] \approx 25 k_{cat}/K_m^{(5)}\ [\text{dsDNA:T7}]\ m$. Hence the effective rate of RNA synthesis (k_5 in our model) is on the order of 2.5×10^5 M^{-1} s^{-1}. For a more detailed discussion of the process see the literature cited and literature therein.

[b] $k_5 = \dfrac{k_{cat}}{K_m}$ for small concentrations.

and the kinetic parameters. The saturation of the enzymes and the exhaustion of resources like primers and nucleotides define a number of titration points separating regimes of different kinetic behavior, as discussed in Ackermann et al. [27] for a coupled system of predator–prey type. These effects have to be taken into account when the concentration of the polynucleotide templates reaches the order of magnitude of the limiting resources in the influx. To simplify the above reaction system we assume the enzymes, primers and dNTP nucleotides are given in excess.

$$\min([\text{P}]_0, [\text{RT}]_0, [\text{T}]_0,\ 4[\text{dNTP}]_0/\nu) > m. \qquad (6)$$

Where the effective nucleotide concentration m is given in units of the RNA concentration which can be synthesized by consuming all ribonucleotide triphosphates (rNTPs). For a chain length of $\nu = 100$ and uniformly distributed nucleotides in the sequence we get $[\text{ATP}]_0 \approx [\text{GTP}]_0 \approx [\text{UTP}]_0 \approx [\text{CTP}]_0 \approx 25\ m_0$. The same applies to the concentration of the deoxyribonucleotide triphosphates (dNTPs). A similar analysis can be applied for other choices of limiting resources. In the following we assume that dNTPs and primers are given in excess. Actually the $[\text{rNTP}]_0$ can be a factor of 10 or more larger and still limiting because approximately 10 times more RNA than DNA is synthesized per primer. The reaction system can be (partly) linearized by setting the corresponding concentration to a constant (the values at time 0) ($[\text{P}_{1,2}] = [\text{P}]_0$, $[\text{RT}] = [\text{RT}]_0$, $[\text{T}] =$

$[T]_0$, and $[dNTP] = [dNTP]_0$) we get the linearized reaction system:

$$
\begin{aligned}
&\mathrm{DNA_1} + \mathrm{DNA_2} \xrightarrow{k_1} \mathrm{DNA_{12}}\\
&\mathrm{DNA_{12}} \xrightarrow{k_2[\mathrm{RT}]_0} \mathrm{DNA_{12}{:}RT}\\
&\mathrm{DNA_{12}{:}RT} \xrightarrow{k_3[\mathrm{dNTP}]_0} \mathrm{dsNDA} + \mathrm{RT}\\
&\mathrm{dsDNA} \xrightarrow{k_4[\mathrm{T}]_0} \mathrm{dsDNA{:}T}\\
&\mathrm{dsDNA{:}T} + M \xrightarrow{k_5} \mathrm{dsDNA} + \mathrm{T} + \mathrm{RNA_1} + \mathrm{RNA_2}\\
&\mathrm{RNA_1} \xrightarrow{k_6[\mathrm{P}]_0} \mathrm{RNA_1{:}P_1}\\
&\mathrm{RNA_2} \xrightarrow{k_6[\mathrm{P}]_0} \mathrm{RNA_2{:}P_2}\\
&\mathrm{RNA_1{:}P_1} \xrightarrow{k_7[\mathrm{RT}]_0} \mathrm{RNA_1{:}P_1{:}RT}\\
&\mathrm{RNA_2{:}P_2} \xrightarrow{k_7[\mathrm{RT}]_0} \mathrm{RNA_2{:}P_2{:}RT}\\
&\mathrm{RNA_1{:}P_1{:}RT} \xrightarrow{k_8[\mathrm{dNTP}]_0} \mathrm{DNA_1} + \mathrm{RT}\\
&\mathrm{RNA_2{:}P_2{:}RT} \xrightarrow{k_8[\mathrm{dNTP}]_0} \mathrm{DNA_2} + \mathrm{RT}.
\end{aligned}
\tag{7}
$$

The new reaction rates of the linearized system will be denoted $\tilde{k}_2 = k_2\,[\mathrm{RT}]_0$, $\tilde{k}_3 = k_3\,[\mathrm{D}]_0$, $\tilde{k}_4 = k_4\,[\mathrm{T}]_0$, etc. The system can simplified further by dropping the indices which distinguish the two symmetric branches: $[\mathrm{RNA_1}] = [\mathrm{RNA_2}] = r$, $[\mathrm{DNA_1}] = [\mathrm{DNA_2}] = d$, $[\mathrm{P_1}] = [\mathrm{P_2}] = p$, etc. The ordinary differential equations (ODE) for the above reaction system can then be written in the form:

$$\frac{\mathrm{d}\vec{C}}{dt} = \mathbf{A}\vec{C} + \vec{f}(\vec{C}). \tag{8}$$

The matrix **A** of effectively first order rate coefficients is given by

$$
\mathbf{A} = \begin{pmatrix}
0 & 0 & 0 & 0 & 0 & 0 & 0 & 0 & +\tilde{k}_8\\
0 & -\tilde{k}_2 & 0 & 0 & 0 & 0 & 0 & 0 & 0\\
0 & +\tilde{k}_2 & -\tilde{k}_3 & 0 & 0 & 0 & 0 & 0 & 0\\
0 & 0 & +\tilde{k}_3 & -\tilde{k}_4 & 0 & 0 & 0 & 0 & 0\\
0 & 0 & 0 & +\tilde{k}_4 & 0 & 0 & 0 & 0 & 0\\
0 & 0 & 0 & 0 & 0 & 0 & -\tilde{k}_6 & 0 & 0\\
0 & 0 & 0 & 0 & 0 & 0 & +\tilde{k}_6 & -\tilde{k}_7 & 0\\
0 & 0 & 0 & 0 & 0 & 0 & 0 & +\tilde{k}_7 & -\tilde{k}_8\\
0 & 0 & 0 & 0 & 0 & 0 & 0 & 0 & 0
\end{pmatrix}
\tag{9}
$$

and describes two chains of linear transformations; one from $\mathrm{DNA_{12}}$ to dsDNA:T and the second from RNA to DNA. In the vector of concentrations $\vec{C}$, the species are ordered as they occur in the above reaction system (7) (except for the monomer m which appears last):

$$
\vec{C} = \begin{pmatrix} d\\ d_{12}\\ d_r\\ d_{\mathrm{ds}}\\ d_t\\ r\\ r_p\\ r_r\\ m \end{pmatrix} := \begin{pmatrix} [\mathrm{DNA}]\\ [\mathrm{DNA_{12}}]\\ [\mathrm{DNA_{12}{:}RT}]\\ [\mathrm{dsDNA}]\\ [\mathrm{dsDNA{:}T}]\\ [\mathrm{RNA}]\\ [\mathrm{RNA{:}P}]\\ [\mathrm{RNA{:}P{:}RT}]\\ M \end{pmatrix}. \tag{10}
$$

The vector of non-linear terms involving template–template hybridization and monomer consumption during transcription:

$$
\vec{f}(\vec{C}) = (-k_1 d^2,\ k_1 d^2,\ 0,\ \mathbf{k_5 d_t m},\ -k_5 d_t m,\ k_5 d_t m,\ 0,\ 0,\ -k_5 d_t m)^T \tag{11}
$$

closes the amplification cycle. The regeneration of double stranded DNA (bold face entry in the vector $\vec{f}$) following transcription is responsible for the net amplification of the cycle. The linear terms of Eq. (8) consist of binding reactions to enzymes and primers (both given in excess) and enzymatic steps of polynucleotide processing.

These two types of reactions take place on very different time scales. These binding steps are fast reactions compared with the enzymatic activities involved in the amplification cycle. This motivates the definition of the lumped concentrations

$$d'_{12} = [\mathrm{DNA}_{12}] + [\mathrm{DNA}_{12}\mathrm{:RT}]$$

$$d'_{\mathrm{ds}} = [\mathrm{dsDNA}] + [\mathrm{dsDNA:T}]$$

$$r' = [\mathrm{RNA}] + [\mathrm{RNA:P}] + [\mathrm{RNA:P:RT}].$$

On the time scale of the enzyme activities, the fast binding reactions can be assumed to be in a steady state and the lumped concentrations are approximated by

$$d'_{12} \approx [\mathrm{DNA}_{12}\mathrm{:RT}]$$

$$d'_{\mathrm{ds}} \approx [\mathrm{dsDNA:T}]$$

$$r' \approx [\mathrm{RNA:P:RT}].$$

The kinetics of the lumped concentrations is described by the reduced ODE

Table 4
List of some kinetic data for the RNA-dependent DNA polymerase function of HIV reverse transcriptase (RT):[a]
$\mathrm{RT} + \mathrm{RNA:P} \overset{K_d^{(4)}}{\rightleftharpoons} \mathrm{RNA:P:RT} \overset{k_{\mathrm{cat}}}{\rightarrow} \mathrm{DNA} + \mathrm{RT}.$

Parameter	Value	References
Dissociation constant for enzyme–template–primer binding		
$K_d^{(4)}$ (nM)	2.5	[53]
	4.7	[51]
	10	[50,54]
	0.44	[55]
	1.0	[59]
Rate constant for association of enzyme–template–primer complex		
k_7 (10^6 M^{-1} s^{-1})	4	[50,54]
	68.2	[55]
	1.0	[59]
	1.5	[100]
Rate constant for dissociation of enzyme–template–primer complex		
k_{-7} (s^{-1})	0.06	[53,51]
	0.04	[50,54]
	0.001	[59]
Dissociation constant for nucleotide binding		
$K_d^{(5)}$ (μM)	9	dTTP [50]
	14	[51,59]
Single nucleotide incorporation		
k_{cat} (s^{-1})	0.012–0.085	[50]
	0.0031	[59]
$\tilde{k}_8$ (s^{-1})	0.04[b]	

[a] *Notes.* Using experimental essays with nucleotides given in excess, most experimental groups found, as for the DNA-directed DNA polymerase of RT, a fast polymerization rate 13–72 nucl/s [50,54,59,51] and the dissociation of the enzyme of the DNA product the rate limiting step. The range of kinetic rate k_{cat} is broad and depends on the experimental conditions. In general the RNA-directed DNA polymerase of RT is slower than the DNA-directed DNA polymerase and we adopt a value of $\tilde{k}_8 = 0.04\ \mathrm{s}^{-1}$ as a standard value for numerical simulations. For a more detailed discussion of the process see the cited literature

[b] Estimated value.

$$\frac{\partial}{\partial t}\begin{pmatrix} d \\ d'_{12} \\ d'_{ds} \\ r'm \end{pmatrix} = \begin{pmatrix} 0 & 0 & 0 & 0 & +\tilde{k}_8 \\ 0 & -\tilde{k}_3 & 0 & 0 & 0 \\ 0 & +\tilde{k}_3 & 0 & 0 & 0 \\ 0 & 0 & 0 & 0 & -\tilde{k}_8 \\ 0 & 0 & 0 & 0 & 0 \end{pmatrix} \times \begin{pmatrix} d \\ d'_{12} \\ d'_{ds} \\ r' \\ m \end{pmatrix} + \begin{pmatrix} -k_1 d^2 \\ +k_1 d^2 \\ 0 \\ +k_5 d'_{ds} \times m \\ -k_5 d'_{ds} \times m \end{pmatrix} \quad (12)$$

corresponding to the following reaction system:

$$\mathrm{DNA}_1 + \mathrm{DNA}_2 \xrightarrow{k_1} \mathrm{DNA}'_{12} \xrightarrow{\tilde{k}_3} \mathrm{dsDNA}'$$

$$\mathrm{dsDNA}' + M \xrightarrow{k_5} \mathrm{dsDNA}' + \mathrm{RNA}'_{1,2} \quad (13)$$

$$\mathrm{RNA}'_{1,2} \xrightarrow{\tilde{k}_8} \mathrm{DNA}_{1,2}.$$

For our numerical simulations, we adopt the kinetic rate constants $k_1 = 10^{7\pm1}$ M^{-1} s^{-1}, $\tilde{k}_3 = 0.1$ s^{-1}, $k_5 = 2.5 \times 10^5$ M^{-1} s^{-1}, and $\tilde{k}_8 = 0.04$ s^{-1} estimated from kinetic data in the literature; the effective nucleotide concentration in the inlet of the flow reactor is set to $m = 10^{-6}$ M (see Tables 1–4).

A further reduction of the reaction system is possible for low template concentrations. In this case, the binding of DNA_1 and DNA_2 will be the rate limiting step in the conversion of single stranded DNA to dsDNA. Thus, dropping the intermediate DNA'_{12} we get:

$$\mathrm{DNA}_1 + \mathrm{DNA}_2 \xrightarrow{k_1} \mathrm{dsDNA}'$$

$$\mathrm{dsDNA}' + M \xrightarrow{k_5} \mathrm{dsDNA}' + \mathrm{RNA}'_{1,2} \quad (14)$$

$$\mathrm{RNA}'_{1,2} \xrightarrow{\tilde{k}_8} \mathrm{DNA}_{1,2}.$$

For a given (fixed) concentration of the double stranded DNA, the steady state value of the RNA concentration is

$$r^* = \frac{k_5 m}{\tilde{k}_8}[\mathrm{dsDNA}']. \quad (15)$$

In this case the reverse transcription rate of RNA to DNA becomes

$$\frac{\mathrm{d[DNA]}}{dt} = k_5 m \ [\mathrm{dsDNA}]. \quad (16)$$

Thus, assuming the production of RNA and its reverse transcription to DNA to be in a steady state, we can drop the intermediate RNA also and get the very simple reaction system

$$\mathrm{DNA}_1 + \mathrm{DNA}_2 \xrightarrow{k_1} \mathrm{dsDNA}$$

$$\mathrm{dsDNA} + M \xrightarrow{k_5} \mathrm{dsDNA} + \mathrm{DNA}_{1,2}. \quad (17)$$

In this section, we successively lumped the concentrations of intermediates to obtain a hierarchy of models with decreasing complexity. A summary of this kinetic hierarchy is shown in Fig. 3. Considering the amplification of polynucleotides in a closed CATCH cycle, however, the concentrations of the intermediates will not reach their steady state values instantaneously. The full reaction system (1–5), for example, shows delayed response of the DNA production rate to changes in the concentration of double stranded DNA. In the small system (17), an increase of the concentration of dsDNA instantaneously leads to an increased production rate of DNA. While inertial features of the full system are not important for the discussion of steady states (in a flow reactor), it is for the dynamical growth of species.

4. Kinetic behavior

Conventional biochemical and organic amplification mechanisms are either exponential [11,66–68] or subexponential (e.g. parabolic [69]). As we shall see below, the critical property of the

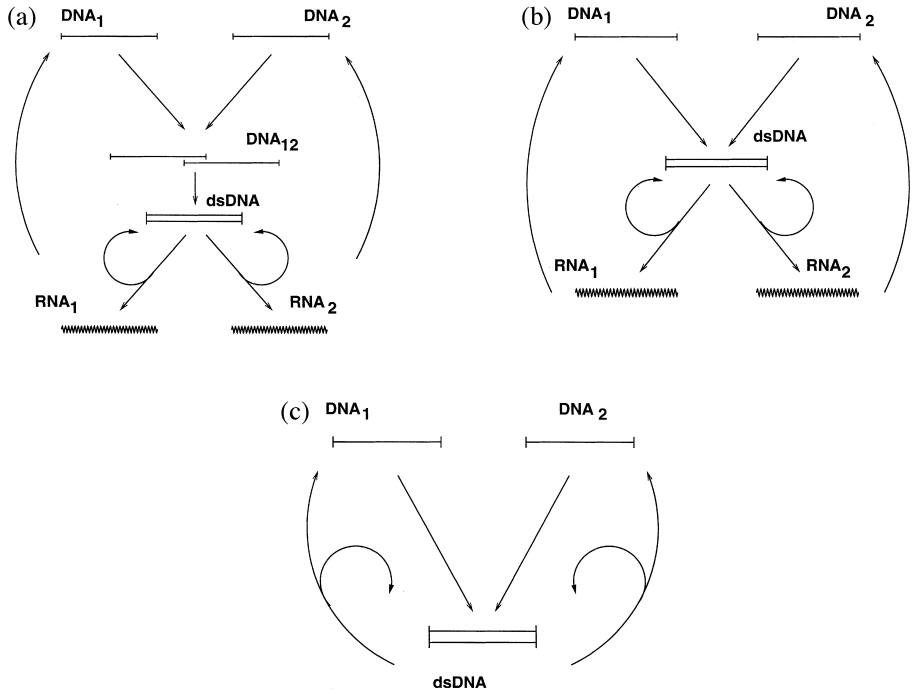

Fig. 3. Reduced reaction mechanism for CATCH: (a) Reduced model of the CATCH system as modeled in the reaction system (13). Enzymes and primers are both given in excess. The binding reactions of enzymes and primers are fast reactions compared with the enzymatic activities involved in the amplification cycle. This motivates the introduction of lumped concentrations [see Eq. (12)]. (b) A further reduction of the reaction system is possible for low template concentrations [Eq. (14)]. In this case, the binding of DNA_1 and DNA_2 will be the rate limiting step in the conversion of single stranded DNA to dsDNA so the intermediate DNA'_{12} is neglected. (c) This scheme shows the simplest model for the CATCH system we investigated (17). Assuming the production of RNA and its reverse transcription to DNA to be in a steady state, we can drop the intermediate RNA. This simple scheme may be compared with other pattern generating mechanisms (see Section 7). The resource M which is consumed in the transcription step from dsDNA to RNA_1 and RNA_2 is not shown in this figure.

kinetics responsible for complex pattern formation in models of self-replicating spots is a greater than linear dependence of the amplification on the concentration (corresponding to hyperexponential growth), at least at low concentrations. That this is the case for CATCH can bee seen from a simplified analysis.

The kinetic behavior of the full reaction system (1–5) and the reduced systems (13), (14) and (17) requires careful analysis. We mentioned above that the system will 'explode' after a finite reaction time, if no depletion of resources or inhibition of enzymes are considered. The differential equation for the simplest reaction system (17) is given by

$$\begin{aligned} \dot{\mathrm{dna}}_1 &= -k_1\ \mathrm{dna}_1\ \mathrm{dna}_2 + k_5\ \mathrm{dsdna}\ m \\ \dot{\mathrm{dna}}_2 &= -k_1\ \mathrm{dna}_1\ \mathrm{dna}_2 + k_5\ \mathrm{dsdna}\ m \\ \dot{\mathrm{dsdna}} &= k_1\ \mathrm{dna}_1\ \mathrm{dna}_2 \\ \dot{m} &= -2k_5\ \mathrm{dsdna}\ m. \end{aligned} \tag{18}$$

The mass conservation gives $\mathrm{dna}_1 + \mathrm{dna}_2 + 2\ \mathrm{dsdna} + m = \text{constant}$. We introduce the concentrations:

$$\begin{aligned} \mathrm{dna}_+ &= \mathrm{dna}_1 + \mathrm{dna}_2 \\ \mathrm{dna}_- &= \mathrm{dna}_1 - \mathrm{dna}_2. \end{aligned} \tag{19}$$

Immediately follows $\mathrm{dna}_- = \text{constant}$ and since the asymmetric case gave no essential new information we concentrate on the symmetric case. Using the abbreviations $x = \mathrm{dna}_+ = \mathrm{dna}_1 + \mathrm{dna}_2$ and $y = 2\ \mathrm{dsdna}$ we get:

$$\dot{x} = -k_1/2x^2 + k_5 m y$$
$$\dot{y} = +k_1/2x^2$$
$$\dot{m} = -k_5 m y. \quad (20)$$

For resources given in excess, we can assume $k_5 m$ to be constant ($m = m_0$, corresponding to the max. Michaelis rate) and for small concentration of single stranded species ($k_1/2\ x^2 \ll k_5 m\, y$) we can approximate the reaction system by:

$$\dot{x} = k_5\, m_0\, y$$
$$\dot{y} = k_1/2x^2. \quad (21)$$

In this case, a solution of the ODEs is given by

$$x = \left(\frac{1}{\sqrt{x_0}} - \sqrt{\frac{k_1 k_5 m_0}{12}}\, t \right)^{-2},$$
$$y = \sqrt{\frac{k_1}{3 m_0 k_5}}\, x^{3/2},$$
$$\dot{x} = \sqrt{\frac{1}{3} k_1 k_5 m_0}\, x^{3/2}. \quad (22)$$

The effective reaction order of $3/2$ in this equation shows the faster than exponential (hyperbolic) growth of the cooperatively coupled system. This reaction is different to the exponent 2 in the Gray–Scott model. The singularity of x at $t = \sqrt{12/(k_1 k_5 x_0 m_0)}$ is a consequence of the artificial approximation of infinite resources ($m = m_0 = \text{constant}$), which is only valid for $x \ll m_0$. The assumption

$$-k_1/2\, x^2 + k_5 m y \approx k_5 m y \quad (23)$$

is only valid for

$$x \ll \frac{m_0 k_5}{3 k_1} \quad (24)$$

which in case of realistic parameters $m_0 = 10^{-6}$ M, $k_5 = 2.5 \times 10^5\ \mathrm{M^{-1}\ s^{-1}}$ and $k_1 = 10^{7\pm1}\ \mathrm{M^{-1}\ s^{-1}}$ gives:

$$x \ll 8.3 \times 10^{-9\pm1}\ \mathrm{M}, \quad (25)$$

Numerical solution for the concentration of double stranded DNA for the full (as given in 7) and the reduced systems (13 and 14) are plotted in Fig. 4. In the simulations primers, enzymes and dNTPs are given in excess so that the rNTPs are the limiting resource. The initial concentrations of $DNA_{1/2}$ and $RNA_{1/2}$ are set to be zero. Each curve starts at low template concentration ($[\mathrm{dsDNA}]_0 = 10^{-8}$ M), grows with increasing reaction time and is limited by the condition

$$[\mathrm{dsDNA}] \le [\mathrm{dsDNA}]_0 + m_0/2 \approx m_0/2 = 5 \times 10^{-7}\ \mathrm{M}.$$

The resource m goes down essentially exponential and x goes to a maximum and then decreases with $1/t$. The qualitative behavior of all curves is very similar and an adaptation to the amplification behavior of the full system is possible by lowering the corresponding (effective) kinetic parameters for the reduced systems. Further simulations have shown that the curves are insensitive to the inclusion of the reverse bimolecular dissociation steps (for primer annealing, DNA–DNA annealing and enzyme binding).

5. Bifurcation analysis

In Sections 3 and 4 we neglected the flow terms. In this section we come back to the non-zero flow case, which is necessary for pattern formation, but concentrate the analysis on a well-stirred flow reactor, neglecting spatial effects. As in Section 4, we start with the simplest system for which a complete analysis is easily possible.

Before proceeding, a short comment on the modeling for the non-zero flow case is appropriate. As we will see later, we are mainly interested in experimental parameter regions where the template concentrations are kept rather low by sufficiently high flow rates. In this case, the vital DNA–DNA binding steps in the CATCH system become very slow and a complete neglect of competitive loss reactions may not be satisfied. Such loss processes are the digestion of the RNA

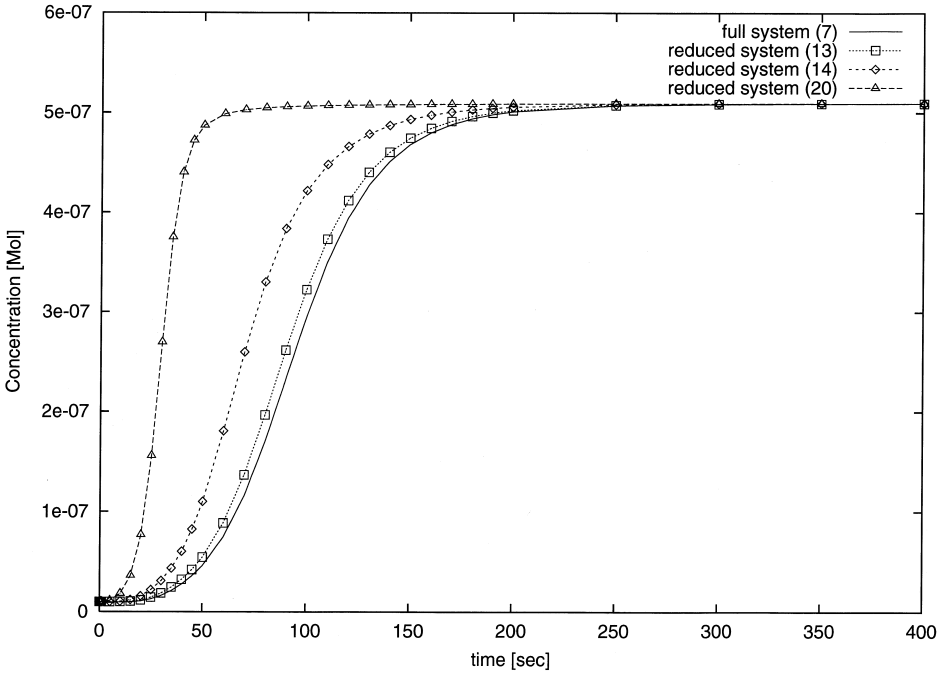

Fig. 4. Numerical solution for the concentration of double stranded DNA for the full (as given in 7) and the reduced (13 and 14) systems. The curves are computed with the kinetic rate constants $k_1 = 10^7\ \mathrm{M}^{-1}\ \mathrm{s}^{-1}$, $k_2 = k_6 = 10^8\ \mathrm{M}^{-1}\ \mathrm{s}^{-1}$, $\tilde{k}_3 = 0.1\ \mathrm{s}^{-1}$, $k_4 = 10^7\ \mathrm{M}^{-1}\ \mathrm{s}^{-1}$, $k_5 = 2.5 \times 10^5\ \mathrm{M}^{-1}\ \mathrm{s}^{-1}$, $k_7 = 10^6\ \mathrm{M}^{-1}\ \mathrm{s}^{-1}$, and $\tilde{k}_8 = 0.04\ \mathrm{s}^{-1}$ estimated from kinetic data in the literature. In the simulations primers, enzymes and dNTPs are given in excess so that the rNTPs (initial concentration: 10^{-6} M) are the limiting resources. The initial concentrations of $\mathrm{DNA}_{1/2}$ and $\mathrm{RNA}_{1/2}$ are set to be zero. Each curve starts at low template concentration $[\mathrm{dsDNA}]_0 = 10^{-8}$ M), grows with increasing reaction time and is limited by the condition $[\mathrm{dsDNA}] \leq [\mathrm{dsDNA}]_0 + m_0/2 \approx m_0/2 = 5 \times 10^{-7}$ M. The qualitative behavior of all curves are very similar and an adaptation to the amplification behavior of the full system is possible by lowering the corresponding (effective) kinetic parameters for the reduced systems. Further simulations have shown that the curves are insensitive to the reversal of the bimolecular association steps (primer annealing, DNA–DNA annealing and enzyme binding).

strands by the RNAse activity of enzymes and numerous binding reactions which lead to non-functional molecules. Only first order loss (or death) reactions will have a significant effect and for the reduced system (20) adding such loss terms gives

$$\begin{aligned} \dot{x} &= -k_1/2\, x^2 + k_5 m y - (F + \mathscr{K}) x \\ \dot{y} &= +k_1/2\, x^2 - (F + \mathscr{K}') y \\ \dot{m} &= -k_5 m y - F(m - m_0). \end{aligned} \tag{26}$$

where $\mathscr{K}$, $\mathscr{K}'$, are effective kinetic parameters which consider possible dead end side-reactions. The resource M is added by a constant influx and all three species are removed by the feed process with rate F.

Of special interest are the steady states and their stability as a function of the free parameters of the system. The number of parameters of the system can be reduced by reexpressing the equations in dimensionless form. Measuring concentrations and time in units of ξ and τ

$$\xi = m_0, \quad \tau = \frac{1}{k_5 m_0} \tag{27}$$

the differential equations read ($x = \xi\tilde{x}$, $y = \xi\tilde{y}$, $m = \xi\tilde{m}$)

$$\begin{aligned} \dot{\tilde{x}} &= -\alpha\, \tilde{x}^2 + \tilde{m}\tilde{y} - (f + \kappa)\tilde{x} \\ \dot{\tilde{y}} &= +\alpha\, \tilde{x}^2 - (f + \kappa')\tilde{y} \end{aligned} \tag{28}$$

$$\dot{m} = -\tilde{m}\tilde{y} + f(1-\tilde{m}).$$

The free parameters are $\alpha = k_1/2k_5$, $f = F\tau$, $\kappa = \mathscr{K}\tau$, and $\kappa' = \mathscr{K}'\tau$. This system has one trivial fixed point for $\tilde{x} = \tilde{y} = 0$ and $\tilde{m} = 1$. The non-trivial fixed points $(\tilde{x}^*, \tilde{y}^*, \tilde{m}^*)$ can easily be computed from:

$$\tilde{y}^* = \frac{\alpha \tilde{x}^{*2}}{f+\kappa'} \quad \tilde{m}^* = \frac{\alpha \tilde{x}^{*2} + (f+\kappa)\tilde{x}^*}{\tilde{y}^*} \tag{29}$$

and the solution of the cubic equation:

$$\tilde{x}^{*3} + A\tilde{x}^{*2} + B\tilde{x}^* + C = 0. \tag{30}$$

with

$$A = \frac{f+\kappa}{\alpha} \quad B = \frac{f(f+\kappa'-1)}{\alpha}$$
$$C = \frac{f(f+\kappa)(f+\kappa')}{\alpha^2}. \tag{31}$$

Since f, κ, and κ' are positive parameters, A and C must be positive too and so physical (non-negative $\tilde{x}^*$) steady state solutions of (30) exists only for negative B, i.e. for $f + \kappa' < 1$. The cubic equation (30) has either zero, one or two positive solutions. The local stability of the fixed points are determined by the eigenvalues of the Jacobian matrix:

$$\mathbf{J} = \begin{pmatrix} -2\alpha\tilde{x}^* - f - \kappa & 2\alpha\tilde{x}^* & 0 \\ \tilde{m}^* & -f-\kappa' & -\tilde{m}^* \\ \tilde{y}^* & 0 & -\tilde{y}^* - f \end{pmatrix} \tag{32}$$

A fixed point of Eq. (28) is unstable if at least one eigenvalue of **J** has a positive real part and stable if all eigenvalues have only negative real parts.

For the sake of simplicity, let us first discuss the case $\kappa' = \kappa$ and $\alpha = k_1/2k_5 = 1$. In this case the only remaining free parameters of the system are the flow rate f and the death rate κ. A bifurcation diagram for the fixed points of this

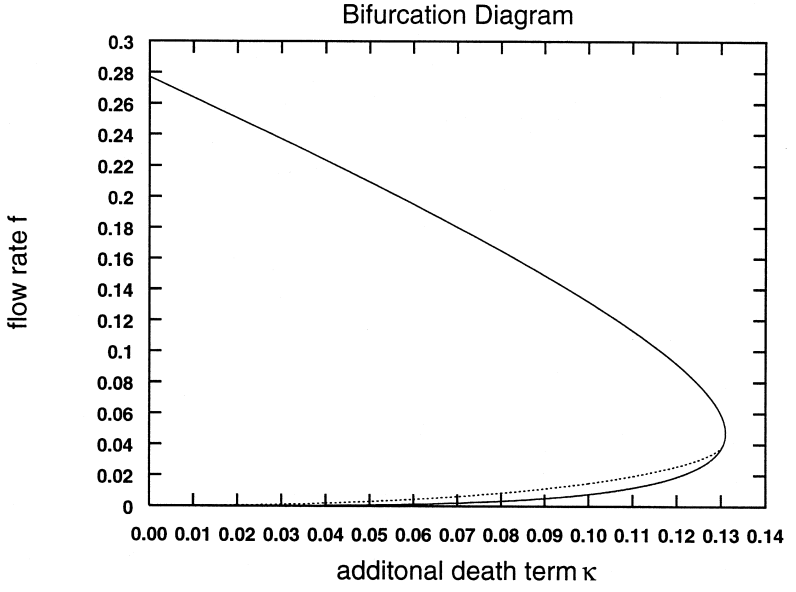

Fig. 5. Bifurcation diagram of the parameter space for the reduced reaction scheme (17) of CATCH. f and κ are the two bifurcation parameters of the system. The dashed line shows the Hopf bifurcation and the solid line the saddle node bifurcation. Outside the region bounded by the solid line, there is a single stable fixed point (the trivial steady state) with the concentrations; $\tilde{x} = \tilde{y} = 0$ and the resource concentration $\tilde{m} = 1$. In the region above the solid line and below the dashed line are two unstable fixed points and the stable trivial steady state. Above the dashed line and below the solid line exist two (one non-trivial stable steady state) and one unstable fixed point. Since two linearly stable steady states exist in this region the system is bistable.

system in the (f, κ) plane is shown in Fig. 5. The trivial steady state exists in the whole (f, κ) plane. Depending on the parameters κ and f, two non-trivial fixed points emerge. The saddle node bifurcation given by the solid line divides the (f, κ) plane up into two regions: one 'inside' region where the two non-trivial fixed points exist and the second 'outside' region where only the trivial steady state exists. The two non-trivial steady states in the 'inside' region are either both unstable or one is stable and the other is unstable. The stable steady state loses its stability for decreasing f by a Hopf bifurcation shown by the dashed line.

Non-trivial fixed points exist for death rates below a critical value $\kappa < \kappa_c$. For each death rate $\kappa < \kappa_c$ there exists a maximal flow rate above which the system is diluted out. This maximal flow rate decreases as the death term κ increases. The combined effect of the dilution by the flow rate and the death term must be low enough to enable an effective growth of the system. The flow term, however, is not only responsible for dilution but also for the input of resources. Thus the system also becomes unstable if the flow rate is too low. This effect becomes pronounced for a large death rate.

Increasing the parameter α (values of $\alpha \gg 1$ follow from the kinetic data in Tables 1–4), the system becomes more stable. The maximal death parameter κ increases as well; the qualitative form of the bifurcation diagram, however, remains unchanged for increasing α. For $\alpha = 200$, for example, the maximal flow rate coefficient is approximately 0.75 and the maximal death parameter is approximately 0.5. Distinguishing between the death term κ and κ' we found a small death parameter κ' (for the double stranded species) to increase the viability of the system.

The bifurcation analysis is also straightforward for the reaction system (13) and (14). Despite the increased complexity in these systems the results are very similar for system (14). Here the parameters F and $\mathscr{K}$ are introduced by adding the terms

$$C \xrightarrow{F+\mathscr{K}} \emptyset \quad \text{for } C \in \{\mathrm{DNA}_{1,2},\ \mathrm{DNA}'_{12},\ \mathrm{dsDNA}',\ \mathrm{RNA}'_{1,2}\}$$

$$\emptyset \xrightarrow{F[M]_0} M$$

$$M \xrightarrow{F} \emptyset.$$

whereas the kinetic parameters are set according to Tables 2–4. Similar results are expected for the full system (7) adding appropriate flow terms.

6. Spatial effects

The reaction–diffusion equation corresponding to the ODE [Eq. (28)] is given in dimensionless form by

$$\begin{aligned}
\dot{\tilde{x}} &= -\alpha \tilde{x}^2 + \tilde{y}\tilde{m} - (f+\kappa)\tilde{x} + d_{\tilde{x}}\nabla^2\tilde{x} \\
\dot{\tilde{y}} &= +\alpha \tilde{x}^2 - (f+\kappa)\tilde{y} + d_{\tilde{y}}\nabla^2\tilde{y} \\
\dot{\tilde{m}} &= -\tilde{y}\tilde{m} + f(1-\tilde{m}) + d_{\tilde{m}}\nabla^2\tilde{m}.
\end{aligned} \tag{33}$$

where the dimensionless spatial coordinate is scaled by the length scale l (adapted to our numerical grid) given by

$$l = \sqrt{\frac{D_{\tilde{m}}}{k_5 m_0 0.1}} \tag{34}$$

For a typical experimental diffusion rate of $D_{\tilde{m}} = 4 \times 10^{-7}$ cm^2 s^{-1} and standard parameters $k_5 = 2.5 \times 10^5\ M^{-1}\ s^{-1}$, $m_0 = 1 \times 10^{-6} M$, the unit of length is $l \approx 40$ μm. The dimensionless diffusion rate d_i is then

$$d_i = \frac{D_i}{k_5 m_0 l^2} \tag{35}$$

and for values listed in Table 1 we obtain $d_{\tilde{m}} = 0.1$, and $d_{\tilde{x}} = d_{\tilde{y}} = 0.05$.

We applied a finite-difference discretization to the diffusion operator and a forward Euler integration to the reaction–diffusion Eq. (33) with periodic boundary conditions. A spatial mesh with 256×256 grid points and time steps of one (in dimensionless units) turned out to be sufficiently fine not to influence the results presented here,

the distance between two grid points being set to one (in dimensionless units). This choice corresponds to a physical reactor size of 1.024×1.024 cm. Initially, the entire system was placed in the trivial steady state ($\tilde{x} = 0$, $\tilde{y} = 0$ and $\tilde{m} = 1$). A 25×25 grid points square in the middle of the array is used to start an initial perturbation with $\tilde{x} = 0.25$, $\tilde{y} = 0.25$ and $\tilde{m} = 0.5$ and then these initial conditions were perturbed with $\pm 1\%$ random noise. We set $\alpha = 1$ in the first instance.

The initial perturbation spreads wave-like over the field with a velocity of 2×10^{-2}. Depending on the parameter values, 10 000–20 000 time steps are required for this case to spread over the entire grid. A simulation time of 200 000 steps is sufficient to reach the asymptotic state of the system. We observed the formation of time dependent patterns and Turing type patterns in a relatively narrow parameter region in the f, κ plane; for a zoom into this region see Fig. 6. The saddle point bifurcation and the Hopf bifurcation are again represented by the solid and dashed lines. At the points in the parameter plane which are marked with a 0, the concentrations $\tilde{x}$ and $\tilde{y}$ drop to zero and homogeneous asymptotic states corresponding to the trivial steady state described above are obtained. Homogeneous asymptotic states emerge also at points which are marked by a number; the numbers give the value of the concentration $\tilde{x}$ in these states. More interesting results were obtained at the points $P1$–$P14$. Here the asymptotic states are time dependent spatial patterns. The corresponding images, taken after 200 000 time steps, are shown in Fig. 7. The patterns $P1$, $P2$ and $P3$ are called chemical turbulence [70] or phase turbulence [71]. In the corresponding homogeneous asymptotic states no stable oscillations exist. Decreasing f further and leaving the direct neighborhood of the Hopf bifurcation, the patterns become more regular. $P4$, $P5$ and $P6$ are growing rings which open up to spiral and worm like patterns; self-replicating-spots [9] arise at $P7$. Turning now to $k = 0.13$ we found lamellar patterns ($P8$–$P11$) near the coalescence point of the Hopf and saddle node bifurcation. Similar stationary patterns were observed experimentally in the iodate-ferrocyanide-sulfite reaction [72]. Lowering f further,

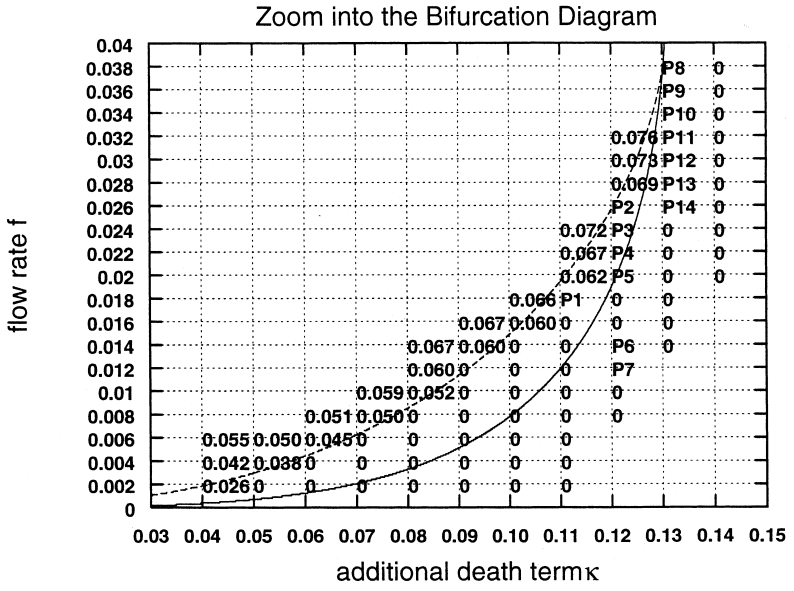

Fig. 6. Blow up of the bifurcation diagram for CATCH shown in Fig. 6. The solid line represents the saddle node bifurcation and the dashed line the Hopf bifurcation. The points marked with $P1$–$P14$ are the points where patterns are found. At the points marked with 0, the system evolves into the trivial steady state. Points marked with numbers indicate non-trivial homogeneous stationary states. The numbers reflect the concentrations of the cooperative species (X).

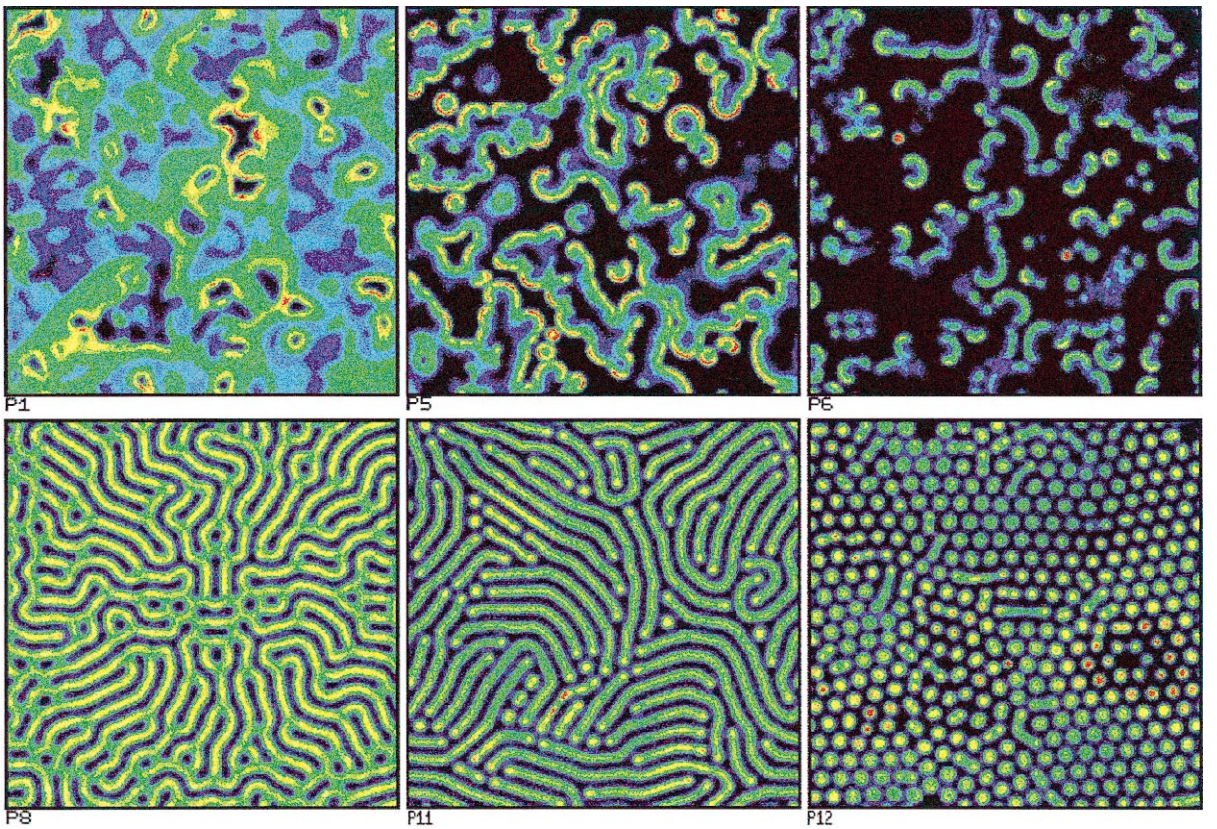

Fig. 7. Some typical patterns of the model [Eq. (33)] with $\alpha = 1.0$. The simulations were performed on a 256×256 point grid. Initially, the entire system was placed in the trivial steady state ($x = 0$, $y = 0$ and $m = 1$). A 25×25 grid point square in the middle of the array is used to start an initial perturbation with $\tilde{x} = 0.25$, $\tilde{y} = 0.25$ and $\tilde{m} = 0.5$ and then these initial conditions were perturbed with $\pm 1\%$ random noise. The diffusion coefficients are $d\tilde{x} = d\tilde{y} = 0.05$ and $d\tilde{m} = 0.1$. The images show the emerged patterns of the partial differential Eq. (33) after 200 000 time steps. The additional death rate κ. and the flow rate f are, from top left to bottom right: $\kappa = 0.11$, $f = 0.018$ ($P1$); $\kappa = 0.12$, $f = 0.02$ ($P5$); $\kappa = 0.12$, $f = 0.014$ ($P6$); $\kappa = 0.13$, $f = 0.038$ ($P8$); $\kappa = 0.13$, $f = 0.032$ ($P11$); $\kappa = 0.13$, $f = 0.03$ ($P12$). The concentration of the variable X is color coded using a rainbow color table: with increasing concentration the color code goes from black ($\tilde{x} = 0$) over violet, blue, light blue, green, light green, yellow to red ($\tilde{x} = 0.1$). The time-dependent pattern $P1$ lies close to the Hopf bifurcation and shows phase or chemical turbulence. Pattern $P5$ and $P6$ are also time-dependent and consists of fledgling spirals that are constantly colliding and annihilating each other. Pattern $P8$ lies next to the coalescence point of the Hopf and the saddle node bifurcation. In a one dimensional simulation in this region, time stable Turing Type patterns were found. Pattern $P8$ and $P11$ resemble those observed experimentally in the iodate-ferrocyanide-sulfite reaction ([72]). The initial perturbation grow radially outward. In the case if two stripes collide, they simply stop (see also [9]). In the time-dependent pattern $P12$ some self-replicating spots may be seen. After the initial perturbation, the spots increase in number until they fill the system. Each spot grows until a critical size in concentration is reached. After a spot has divided to form two spots, they move away from each other. Once the system is filled with spots, they can die due to overcrowding.

self-replicating spots arise ($P12$–$P14$). To show the transitions among the different patterns, varying parameters f and κ, a numerical simulation of the simplest model (17) in a parameter gradient was performed (Fig. 8).

Simulation in one space dimension shows similar pattern formation behavior. Patterns like phase turbulences, self replicating pulses, and Turing patterns were observed for parameter values similar to those for which the corresponding two dimensional patterns emerge. As an example, see the self replicating pulses in Fig. 9. Similar pattern formation behavior has been obtained in simulations with $\alpha = 200$ and for system (14).

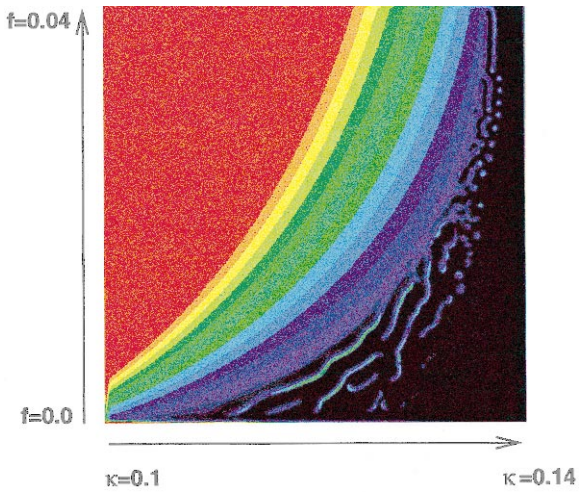

Fig. 8. Numerical calculation of the model [Eq. (33) with an $\alpha = 1.0$] in a gradient of the two parameters f and κ. Space is separated into 512×512 grid points. Calculation was done with a time step of 1.0 and the image was taken after 200 000 time steps. The diffusion coefficients are $d\tilde{x} = d\tilde{y} = 0.05$ and $d\tilde{m} = 0.1$. The concentration of the cooperative species X is color coded using a rainbow color table as in Fig. 7. The maximum value of X is approximately 0.3 (highest non-trivial fixed point). Periodic boundary conditions were used. The space discretization is too coarse to show details of the patterns formed in certain parameter regions, but the figure shows the transitions between the different patterns upon varying parameters f and κ. It should be noted that some patterns result from the periodic boundary conditions (left bottom corner) and may also emerge due to the gradient of the parameters f and κ.

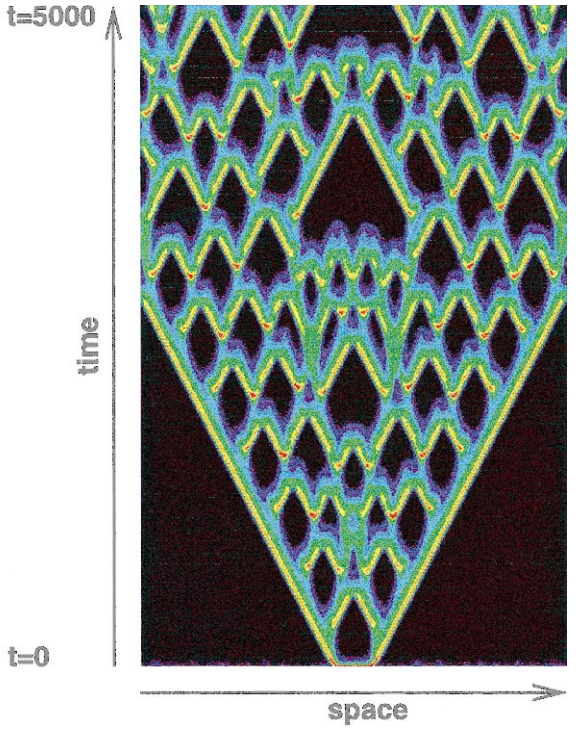

Fig. 9. Numerical calculation of the model [Eq. (33) with $\alpha = 1.0$) in one space dimension (256 grid points). The calculation was done with a time step of 0.5 and the image was taken after 10 000 time steps representing a time of 5000 time units. The additional death term, the flow rate and the diffusion coefficients are $f = 0.22$, $\kappa = 012$, $d\tilde{x} = d\tilde{y} = 0.05$ and $d\tilde{m} = 0.1$, respectively. Periodic boundary conditions are applied. A 20 grid points line in the middle of the array is used to start an initial perturbation with $\tilde{x} = 0.25$, $\tilde{y} = 0.25$ and $\tilde{m} = 0.5$. The symmetry of the initial conditions were destroyed by $+1\%$ random noise. Two pulses emerge from the initial perturbation in the middle of the grid and move away from each other. Each growing pulse divides after approximately 400 time units into two pulses. Two colliding pulses interact strongly and may annihilate one another. The pattern of dividing and colliding pulses spreads over the grid until the domain is filled. Pulses can die due to overcrowding.

These patterns do not appear to emerge from small inhomogeneities in the linearly unstable homogeneous steady state, which would be the characteristic of the bifurcation mechanism proposed by Turing. In our simulations, the initial data are local large-amplitude perturbations from the trivial steady state. The pattern formation occurs in regions in the parameter space where only the trivial fixed point exists. The linear stability of this fixed point against emerging Turing modes is determined by the eigenvalue of the shifted Jacobian

$$\mathbf{J} - k^2\mathbf{D}. \tag{36}$$

D is the diagonal diffusion matrix. It is easy to show that no instability occurs for any real value of the chemical wavelength k. The shift of the Jacobian corresponds to an effective shift of the parameters f and κ and since the trivial fixed point is stable in the whole f, κ plane, it remains stable against Turing modes for each choice of k^2. This means that the steady state solution is linearly stable against the emergence of a single Turing mode. Nevertheless, several patterns obtained in our simulations seem to have one (or

several) intrinsic chemical wave lengths. One-dimensional simulations, for example, show stable Turing patterns each with three different chemical wavelengths near the coalescence point of Hopf and saddle node bifurcation. A detailed analysis in terms of the non-linear evolution equation for the amplitudes of such modes, the generalized Ginzburg–Landau equation [73], lies outside the scope of this paper.

7. Discussion

The CATCH amplification reaction serves as an in vitro experimental model system to investigate the evolution of molecular cooperation. It could be shown that under certain conditions it is possible to reduce the CATCH system to a small model system with only three variables. Numerical simulations of the corresponding partial differential equations exhibit the potential for pattern formation of this model system. Especially the self replicating spot patterns which are known to stabilize such systems against emerging parasites [74,28,30] are of interest. The size of these spots lies in the range of 560–800 μm (the reference length of the calculation is 40 μm) which would be easy to detect in experimental investigations. The range of the concentration depends on the resource. In our case with $m_0 = 1 \times 10^{-6}$ we calculated for the readily experimentally detectable double stranded DNA a concentration variation of 1×10^{-6} M in the center to approximately 5×10^{-9} M at the edge of a spot.

A coupled system based on a predator–prey interaction has also been developed experimentally [23] based on the 3SR reaction. Due to its ability to oscillate [27], the predator–prey system may show pattern formation in a spatial (2D/3D) flow reactor. The mechanism of pattern formation in oscillating predator–prey systems, however, is very different to the possible pattern formations in a trans-cooperatively coupled system shown in this work. In the model of the trans-cooperatively coupled system, patterns were found in a region where the homogeneous system has only the trivial steady state. This fixed point is linearly stable and globally attracting. As indicated by the similarities of the bifurcation diagrams as well as the patterns in the two-dimensional simulations [9], the behavior of the system is strongly reminiscent of the Gray–Scott model [75]

$$U + V + V \rightarrow V + V + V$$
$$V \rightarrow$$

which is described in terms of two species U and V, but includes an (artificial) reaction step of third order. Simulations of the Gray–Scott model in a two-dimensional reaction–diffusion system show complex patterns in certain regions of the f, κ plane [9]. Mathematically it is well known that three component models which show Hopf bifurcation exist having at most bimolecular chemical reactions. A three species model with only one quadratic term showing Hopf bifurcation was recently presented by Wilhelm and Heinrich [76,77]. According to their definition of smallness, their system is the 'smallest' chemical reaction system with Hopf bifurcation. From the viewpoint of chemical intuition or number of parameters, the reduced model (17) for the biochemical CATCH system is simpler however. Whereas the Gray–Scott model consists of two chemical species and contains a reaction step of the third order, the minimal model of CATCH needs three species and only second order reaction steps. The third order reaction in the Gray–Scott model, of course, is an artificial reaction step. A more complicated (enzymatic) reaction system including only second order steps which in some limit (fast reaction steps, Michaelis–Menten kinetics) reduces to the Gray–Scott model shows a similarly complex pattern formation [74,28]. The minimal model of CATCH belongs to a class of small reaction systems which show complex pattern formation and do not contain an artificial third order reaction step. For a similar model [78–80] a transformation to the Gray–Scott model is possible. It has been shown that self-replicating spots are able to stabilize an evolving chemical system against parasites [74,28,30]. The study of self-replicating spot patterns has been the focus of much research activity in previous years [81–84] and references therein. This scenario can be described as a Tur-

ing–Hopf mixed mode [85,86]. A heuristic explanation is given by Reynolds et al. [87] and for a more rigorous investigation we refer to Doelman et al. [88]. A stabilization against parasites due to self-replicating spots, however, cannot be shown without artificial assumptions for continuous reaction–diffusion equations.

In such equations, the parasite concentration cannot become exactly zero at any space point. Emerging parasites are initially in such small concentrations that mass action kinetics does not apply. Either an artificial cutoff value for the concentration of the parasites may be introduced, to describe space regions free of parasites [30], or more realistically a full stochastic model of interacting and diffusing molecules has to be applied (see below).

Furthermore, an experimental system of amplifying DNA/RNA in a two-dimensional flow reactor will undergo a continuous process of mutation and selection, leading to a diversity of individual molecules. The sequences of the individual molecules determine their structural stability, relative binding rates and special functions like promotors or binding sites. New reaction pathways may also evolve and the processed information coded in the sequences of the population determine the kinetic behavior of the system. For CATCH, pattern formation appears only in a narrow region of the parameter space and evolution is easily capable of driving the system outside this region. Outside this region, however, the system is not stable against parasites and the system will be killed by them. This effect may dynamically push the system back into the parameter region where pattern formation emerges. The interaction of evolution, parasites and pattern formation will lead to interesting experimental effects in two-dimensional flow reactors. To study such scenarios stochastically we have developed a simulation platform [29] for the implementation on a massively parallel computer NGEN with configurable hardware [89]. Such a stochastic treatment of CATCH led to similar self-replicating spots (and other patterns) [89]; a detailed description of stochastic simulations of CATCH will be presented in a separate paper. Even with equal diffusion coefficients, stochastic pattern formation in CATCH has been found to appear [90].

Evolutionary studies of serial transfer amplification reactions under batch conditions for the CATCH system have been presented in Ellinger et al. [44]. At low concentration, amplification over a non-cooperative mechanism occurs and at higher concentrations cooperative amplification is preferred. Evolution studies on laboratory time scales are rendered possible by such experiments, so that it is possible to test the tenants of evolutionary population ecology in chemical terms. In order to minimize the cost of such experiments, micro-structured flow reactors [91] with immobilized enzymes (personal communication K. Schmidt) have been designed and produced in our laboratory. Detection of the systems takes place during the reaction using fluorescence spectroscopy based on intercalating dyes and a sequence specific detection method [92,93]. First experiments relating to the measurements of diffusion coefficients and detection of reaction waves have been carried out successfully [22] and we anticipate the first results of pattern formation of evolving biochemical amplification cycles in open spatially resolved reactors in the near future.

Acknowledgements

We thank Thomas Ellinger and Petra Foerster for discussion. This work was supported by grants from the German Ministry of Education, Science and Technology (BMBF, grant no. 0310799).

References

[1] A.M. Turing, Philos. Trans. R. Soc. B 237 (1952) 37.
[2] B.P. Belousov, Sborn. Referat. Radiat. Med, Medgiz, Moscow, 1959, p. 145.
[3] A. M. Zhabotinskii, Biofizika 9 (1964) 306.
[4] V. Castets, E. Dulos, J. Boissonade, P. DeKepper, Phys. Rev. Lett. 64 (1990) 2953.
[5] Q. Ouyang, H.L. Swinney, Nature 352 (1991) 610.
[6] R. Imbihl, G. Ertl, Chem. Rev. 95 (1995) 697.
[7] R. Kapral, K. Showalter (Eds.), Chemical Waves and Patterns, Dordrecht, Kluwer, 1995.
[8] K.J. Lee, W.D. McCormick, J.E. Pearson, H.L. Swinney, Nature 369 (1994) 215.
[9] J.E. Pearson, Science 261 (1993) 189.

[10] S. Spiegelmann, Q. Rev. Biophys. 4 (1971) 213.
[11] G.T. Walker, M.C. Little, J.G. Nadeau, D.D. Shank, Proc. Natl. Acad. Sci. USA 89 (1992) 392.
[12] D.Y. Kwoh, G.R. Davis, K.M. Whitefield, H.L. Chappelle, L. DiMichele, T.R. Gingeras, Proc. Natl. Acad. Sci. 86 (1989) 1173.
[13] J.C. Guatelli, K.M. Whitefield, K.J.B. Deborah, Y. Kwoh, D.D. Richman, T.R. Gingeras, Proc. Natl. Acad. Sci. 87 (1990) 1874.
[14] E. Fahy, D.Y. Kwoh, T.R. Gingeras, PCR Methods Appl. 1 (1991) 25.
[15] R.K. Saiki, S. Scharf, F.A. Faloona et al., Science 230 (1985) 1350.
[16] K.B. Mullis, F.A. Faloona, Methods Enzymol. 155 (1987) 335.
[17] G. von Kiedrowski, Ang. Chem. Int. Ed. Eng. 25 (1986) 932.
[18] J.I. Hong, Q. Feng, V. Rotello, J. Rebek, Jr., Science 255 (1992) 848.
[19] D. Lee, K. Severin, Y. Yokobayashi, M.R. Ghadiri, Nature 390 (1997) 591.
[20] G.J. Bauer, J.S. McCaskill, H. Otten, Proc. Natl. Acad. Sci. USA 86 (1989) 7937.
[21] J.S. McCaskill, G.J. Bauer, Proc. Natl. Acad. Sci. USA 90 (1993) 4191.
[22] A. Bochmann, Diploma thesis, Friedrich-Schiller-Universität Jena, Germany, 1997.
[23] B. Wlotzka, J.S. McCaskill, Biol. Chem. 4 (1997) 25.
[24] R. Ehricht, T. Ellinger, J.S. McCaskill, Eur. J. Biochem. 243 (1997) 358.
[25] J.S. McCaskill, Biophys. Chem. 66 (1997) 145.
[26] Q. Ouyang, Z. Noszticzius, H.L. Swinney, J. Phys. Chem. 96 (1992) 6773.
[27] J. Ackermann, B. Wlotzka, J.S. McCaskill, Bull. Math. Biol. 60 (1998) 329.
[28] J.S. McCaskill, in: P. Schuster (Ed.), Antrittsvorlesungen 1994 an der Friedrich-Schiller Universität Jena, Institut für Molekulare Biotechnologic eV, Jena, Germany, 1995, pp. 27–40.
[29] J.S. McCaskill, U. Tangen, J. Ackermann, in: P. Husband, I. Harvey (Eds.), Fourth European Conference on Artificial Life (ECAL), MIT Press/Bradford Books, Cambridge, MA, 1997, pp. 398–406.
[30] M.B. Cronhjort, C. Blomberg, Physica D 101 (1997) 289.
[31] S. Wright, Proc. VI Int. Cong. Genet. 1 (1932) 356.
[32] S. Wright, Ecology 26 (1945) 415.
[33] M. Kimura, Proc. Natl. Acad. Sci. USA 80 (1983) 6317.
[34] K. Aoki, J. Math. Biol. 25 (1998) 453.
[35] F.J. Dyson, J. Mol. Evol. 118 (1982) 344.
[36] E. Szathmary, Trends Ecol. Evol. 4 (1989) 200.
[37] M. Eigen, Naturwissenschaften 58 (1971) 465.
[38] S.A. Kauffman, J. Cybern. 13 (1971) 71.
[39] O.E. Rössler, Z. Naturforsch. 26b (1971) 741.
[40] M. Eigen, P. Schuster, Naturwissenschaften 11 (1977) 541.
[41] J. Maynard Smith, Nature 280 (1979) 445.
[42] C. Bresch, U. Niesert, D. Harnasch, J. Theor. Biol. 85 (1980) 399.
[43] M.C. Boerlijst, P. Hogeweg, Physica D 48 (1991) 17.
[44] T. Ellinger, R. Ehricht, J.S. McCaskill, Chem. Biol. 5 (1998) 729.
[45] J. Compton, Nature 350 (1991) 91.
[46] J.W. Romano, R.N. Shurtliff, M.G. Sarngadharan, R. Pal, J. Viron. Methods 54 (1995) 109.
[47] R.R. Breaker, G.F. Joyce, Proc. Natl. Acad. Sci. USA 91 (1994) 6093.
[48] C. Majumdar, J.A. Abbotts, S. Broder, S.H. Wilson, J. Biol. Chem. 263 (1988) 15657.
[49] L.V. Mendelman, J. Petruska, M.F. Goodmann, J. Biol. Chem. 265 (1990) 2338.
[50] J.E. Reardon, Biochemistry 31 (1992) 4473.
[51] W.M. Kati, K.A. Johnson, L.F. Jerva, K.S. Anderson, J. Biol. Chem. 267 (1992) 25988.
[52] V. Gopalakrishnan, J.A. Peliska, S.J. Benkovic, Proc. Natl. Acad. Sci. USA 89 (1992) 10763.
[53] H. Yu, M.F. Goodman, J. Biol. Chem. 267 (1992) 10888.
[54] J.E. Reardon, J. Biol. Chem. 268 (1993) 8743.
[55] J.J. DeStefano, R.A. Bambara, P.J. Fay, Biochemistry 32 (1993) 6908.
[56] J.C. Hsieh, S. Zinnen, P. Modrich, J. Biol. Chem. 268 (1993) 24607.
[57] M. Bakhanashvili, A. Hizi, Biochemistry 33 (1994) 12222.
[58] W.A. Beard, S.J. Stahl, H.R. Kim et al., J. Biol. Chem. 269 (1994) 28091.
[59] J.M. Lanchy, C. Ehresmann, S.F.J.L. Grice, B. Ehresmann, R. Marquet, EMBO J. 15 (1996) 7178.
[60] C.T. Martin, J.E. Coleman, Biochemistry 26 (1987) 2690.
[61] D.K. Muller, C.T. Martin, J.E. Coleman, Biochemistry 27 (1988) 5763.
[62] M. Maslak, C.T. Martin, Biochemistry 32 (1993) 4281.
[63] M. Maslak, C.T. Martin, Biochemistry 33 (1994) 6918.
[64] C. Schick, C.T. Martin, Biochemistry 34 (1995) 666.
[65] M. Chamberlin, J. Ring, J. Biol. Chem. 248 (1973) 2235.
[66] C.K. Biebricher, M. Eigen, J.W.C. Gardiner, Biochemistry 22 (1983) 2544.
[67] C.K. Biebricher, M. Eigen, J.W.C. Gardiner, Biochemistry 23 (1984) 3186.
[68] M. Gebinoga, F. Oehlenschläger, Eur. J. Biochem. 235 (1996) 256.
[69] G. von Kiedrowski, Biorgan. Chem. Front. 3 (1993) 113.
[70] O.E. Rössler, Z. Naturforsch. 31a (1976) 1168.
[71] Y. Kuramoto, Chemical Oscillations, Waves and Turbulence, 1st ed., Springer, Berlin, 1984.
[72] K. Lee, W.D. McCormick, Q. Ouyang, H.L. Swinney, Science 261 (1993) 192.
[73] H. Haken, Synergetics. An introduction, Springer, Berlin, 1983.
[74] B. Böddeker, Diploma thesis, Universität Göttingen, Germany, 1995.
[75] P. Gray, S.K. Scott, J. Phys. Chem. 89 (1985) 22.
[76] T. Wilhelm, R. Heinrich, J. Math. Chem. 17 (1995) 1.
[77] T. Wilhelm, R. Heinrich, J. Math. Chem. 19 (1996) 111.

[78] F. Baras, J.E. Pearson, M.M. Mansour, J. Chem. Phys. 93 (8) (1990) 5747.
[79] J.Q. Fang, J.E. Pearson, M.M. Mansour, Comm. Theor. Phys. 17 (1) (1992) 39.
[80] F. Baras, M.M. Mansour, J.E. Pearson, J. Chem. Phys. 105 (18) (1996) 8257.
[81] C.B. Muratov, Phys. Rev. E 54 (1996) 3369.
[82] C.B. Muratov, V.V. Osipov, Phys. Rev. E 54 (1996) 4860.
[83] J.P. Voroney, A.T. Lawniczak, R. Kapral, Physica D 99 (1996) 303.
[84] E. Dulos, P. Davies, B. Rudovics, P.D. Kepper, Physica D 98 (1996) 303.
[85] A.D. Witt, G. Dewel, P. Borckmans, Phys. Rev. E 48 (1993) 4191.
[86] P. Strasser, O.E. Rössler, G. Baier, J. Chem. Phys. 104 (1996) 9974.
[87] W.N. Reynolds, J.E. Pearson, S. Ponce-Dawson, Phys. Rev. Lett. 72 (1994) 2797.
[88] A. Doelman, T.J. Kaper, P.A. Zegeling, Nonlinearity 10 (1997) 523.
[89] J.S. McCaskill, T. Maeke, U. Gemm, L. Schulte, U. Tangen, Lect. Note. Comp. Sci, vol 1259, Springer Verlag, 1997, p. 260.
[90] J. Breyer, J. Ackermann, J.S. McCaskill, Artificial Life 4 (1998) 25.
[91] K. Schmidt, P. Foerster, A. Bochmann, J.S. McCaskill, in: Microreaction Technology, Proceedings of the First International Conference on Microreaction Technology, Springer, Berlin, 1998, pp. 234–244.
[92] S. Tyagi, F.R. Kramer, Nat. Biotech. 14 (1996) 303.
[93] R. Ehricht, T. Kirner, T. Ellinger, P. Foerster, J.S. McCaskill, Nucl. Acids Res. 25 (1997) 4697.
[94] L.E. Morrison, L.M. Stols, Biochemistry 32 (1993) 3095.
[95] R. Ehricht, Ph.D. thesis, Friedrich-Schiller-Universität Jena, Germany, 1998.
[96] M. Kruhøffer, C. Urbanke, F. Grosse, Nucl. Acids Res. 21 (1993) 3943.
[97] S.I. Gunderson, K.A. Chapman, R.R. Burges, Biochemistry 26 (1987) 1539.
[98] A. Újvári, C.T. Martin, Biochemistry 35 (1996) 14574.
[99] H. Aurup, D.M. Williams, F. Eckstein, Biochemistry 31 (1992) 9636.
[100] P. Schwille, F. Ochlenschläger, N.G. Walter, Biochemistry 35 (1996) 10182.